Supplemental Material

Journal of Climate
Two Leading Modes of Wintertime Atmospheric Circulation Drive the Recent Warm Arctic–Cold Eurasia Temperature Pattern
https://doi.org/10.1175/JCLI-D-19-0403.1

Journal of Climate

Supporting Information for

Two leading modes of wintertime atmospheric circulation drive the recent warm Arctic-cold Eurasia temperature pattern

Kunhui Ye[1, 2] and Gabriele Messori[2, 3]

[1]Alfred-Wegener-Institut Helmholtz-Zentrum für Polar- und Meeresforschung, Bremerhaven, Germany

[2]Department of Earth Sciences, Uppsala University, Uppsala, Sweden

[3]Department of Meteorology, Stockholm University, Stockholm, Sweden

Contents of this file

Texts S1-S5

Figures S1-S7

Introduction

The supporting information provides an EOF analysis of the geopotential height at 500 hPa (Z500) for winter (December, January and February) over a larger domain (10°S-90°N, 120°W-160°E). An EOF analysis of Z500 for winter over a similar domain as in Fig. 1 using the NASA MERRA-2 reanalysis is also provided. The supporting information further displays the composite results analogous to Figs. 9 and 10 using filtered daily data. Regression coefficients of the Z500 anomaly for both autumn (September, October and November) and winter against the standardized winter Barents-Kara Sea (BKS) sea-ice are also shown.

Text S1

An EOF analysis of the winter Z500 over 10°S-90°N, 120°W-160°E is performed for comparison with that over 20-90°N, 90°W-160°E from the ERA-Interim reanalysis. As can be seen from Fig. S1, the EOF spatial patterns, resembling respectively an AO-like pattern (Fig. S1a) and a mid-high latitude wave pattern (Fig. S1c), are similar to those of Figs. 1a and 1c in the main text. The principal components (PCs) of both EOF modes are also similar to those of Figs. 1b and 1d in the main text, with correlation coefficients close to 1. The EOF analysis is thus not sensitive to reasonable domain changes.

Text S2

An EOF analysis of the winter Z500 over 20-90°N, 90°W-160°E with the NASA MERRA-2 reanalysis is performed for comparison with that from the ERA-Interim reanalysis. Note that the time period considered for the NASA MERRA-2 reanalysis starts one year later than for ERA-Interim (1981-2017). As can be seen from Fig. S2, the EOF spatial patterns, resembling respectively an AO-like pattern (Fig. S2a) and a mid-high latitude wave pattern (Fig. S2c), are similar to those of Figs. 1a and 1c in the main text. The principal components (PCs) of both EOF modes are also similar to those of Figs. 1b and 1d in the main text, with correlation coefficients close to 1. These results demonstrate that the DJF Z500 EOF modes are robust to the choice of dataset.

Text S3

The daily Z500-projection indices for (a) Z500-PC1 and (b) Z500-PC2 averaged over all positive events are depicted in Fig. S3. The definition of the positive events is given in the main text. Indices are normalised with respect to their individual standard deviations. Day 0 is defined as the day with the maximum index value. Dashed lines denote one standard deviation above/below the mean. As can be seen in the figure, Day 0 as defined in this study can be considered as the peak of the events.

Text S4

The composite results in Figs. S4 and S5 are based on the same procedures as the composite results in Figs. 9 and 10 in the main text. The only difference is that the seasonal-mean is removed from each winter and a Butterworth bandpass filter is applied to retain the 3-90 day band in the daily data before constructing the composite anomalies. This effectively removes variability at longer timescales, including the interannual variability. Comparisons of Figs. S4 and S5 with Figs. 9 and 10 indicate that the spatial patterns are consistent across timescales and there are no obvious qualitative differences. This also suggests that the intraseasonal structures of the two atmospheric circulation modes identified in our study are not overly affected by the trends in the circulation modes in recent decades.

Text S5

The regression results in Fig. S7 suggest that the circulation anomalies associated with both autumn and winter sea-ice anomalies in the BKS region are similar. In particular, the anticyclonic anomaly over the BKS region and North Russia is persistent from autumn to winter. These results suggest that winter circulation anomalies associated with the winter BKS sea-ice could be a result of atmospheric anomaly persistence. Moreover, the circulation anomalies in both seasons are different from those of both the circulation modes defined in the present study. This is consistent with the observation of weak relationships between the winter BKS sea-ice and the two circulation modes in the present study.

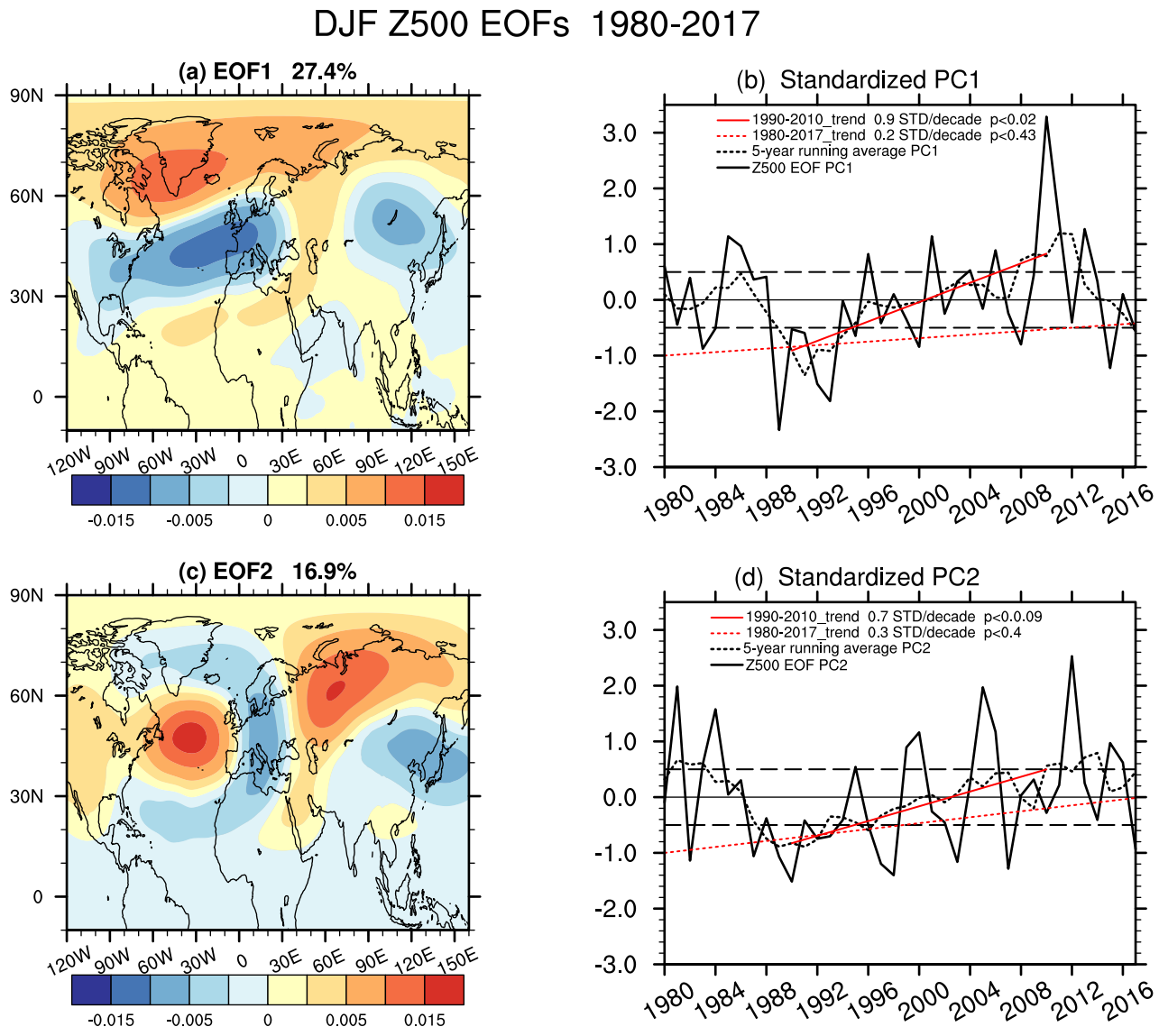

Figure S1. As in Figure 1, but over a larger domain which extends westward and southward.

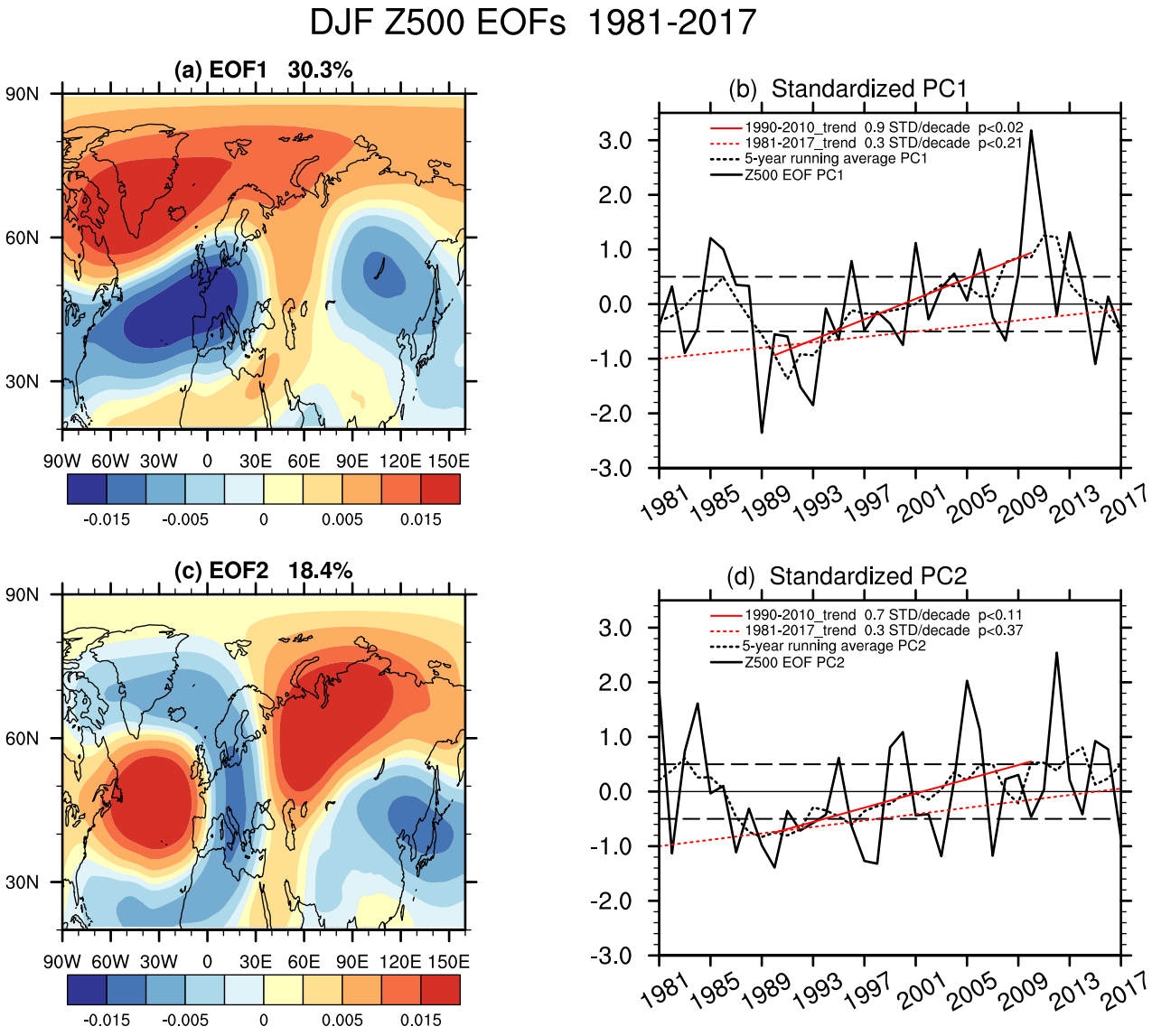

Figure S2. As in Figure 1, but using the NASA MERRA-2 reanalysis

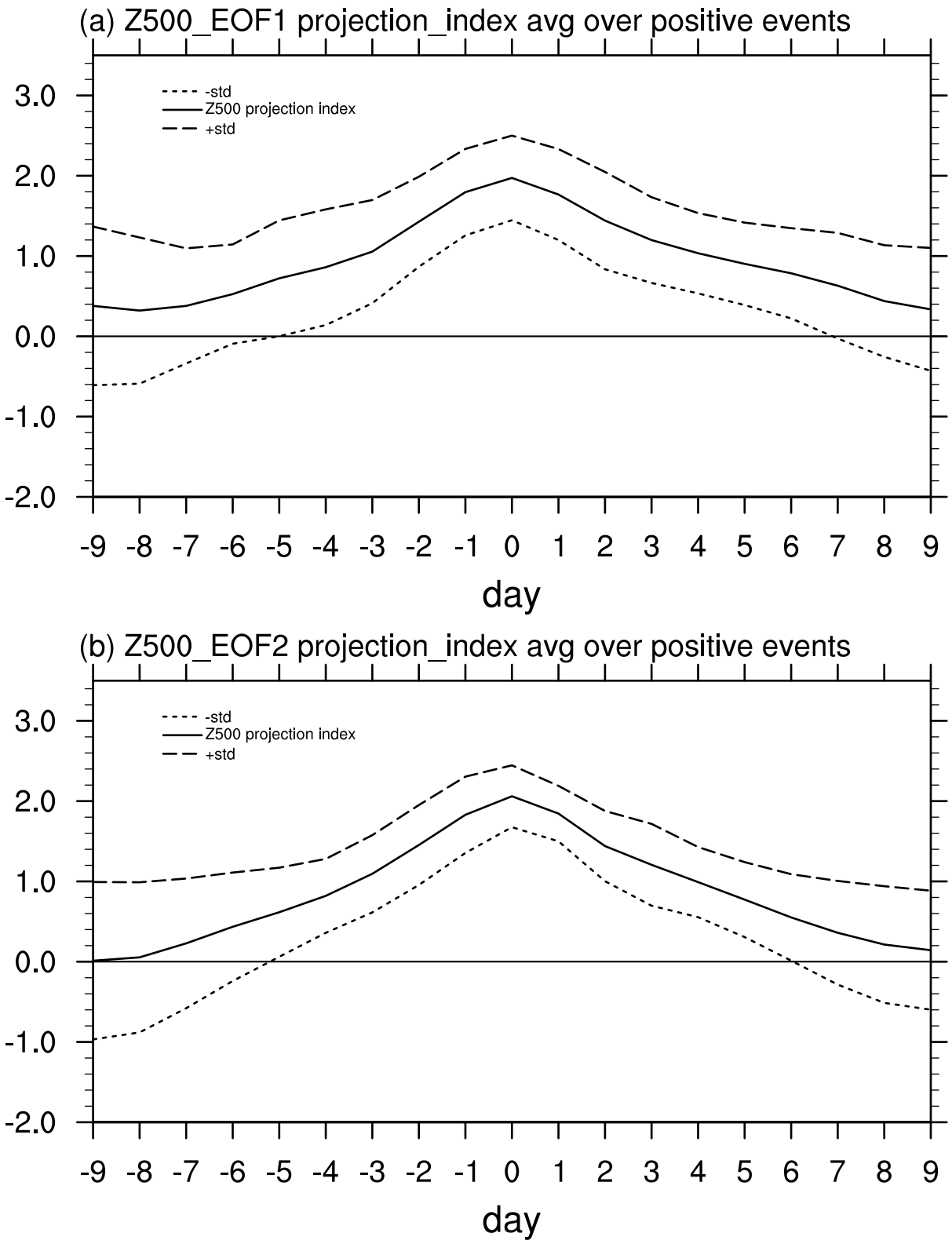

Figure S3. Daily Z500-projection indices for (a) Z500-PC1 and (b) Z500-PC2 averaged over all identified positive events. The daily indices are normalised against their standard deviations. The day number is determined against the day with maximum index value (i.e., day 0). Dashed lines denote one standard deviation above/below the mean.

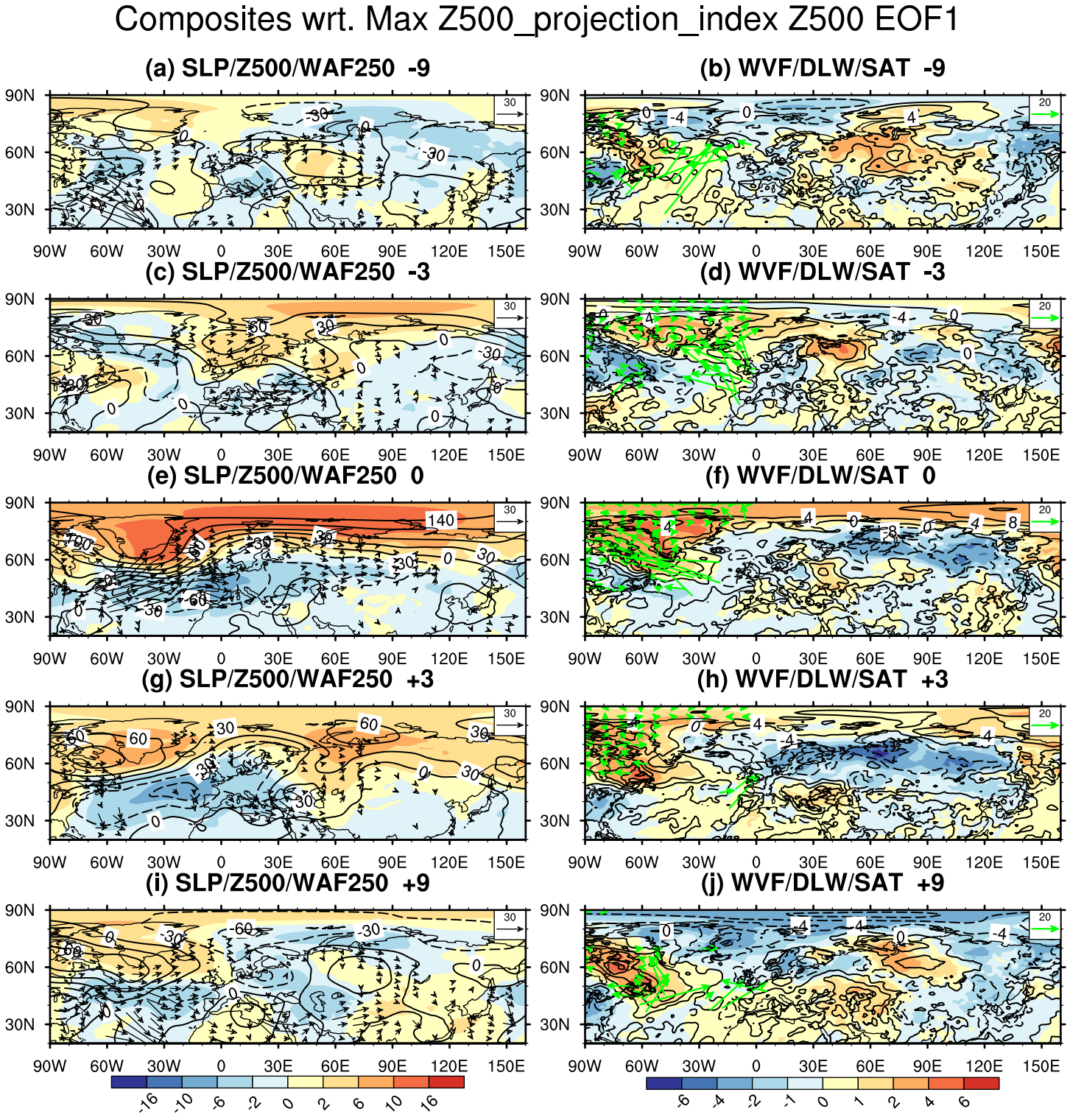

Figure S4. As in Figure 9, but using the filtered daily data. The seasonal-mean mean is also removed from each winter in the data.

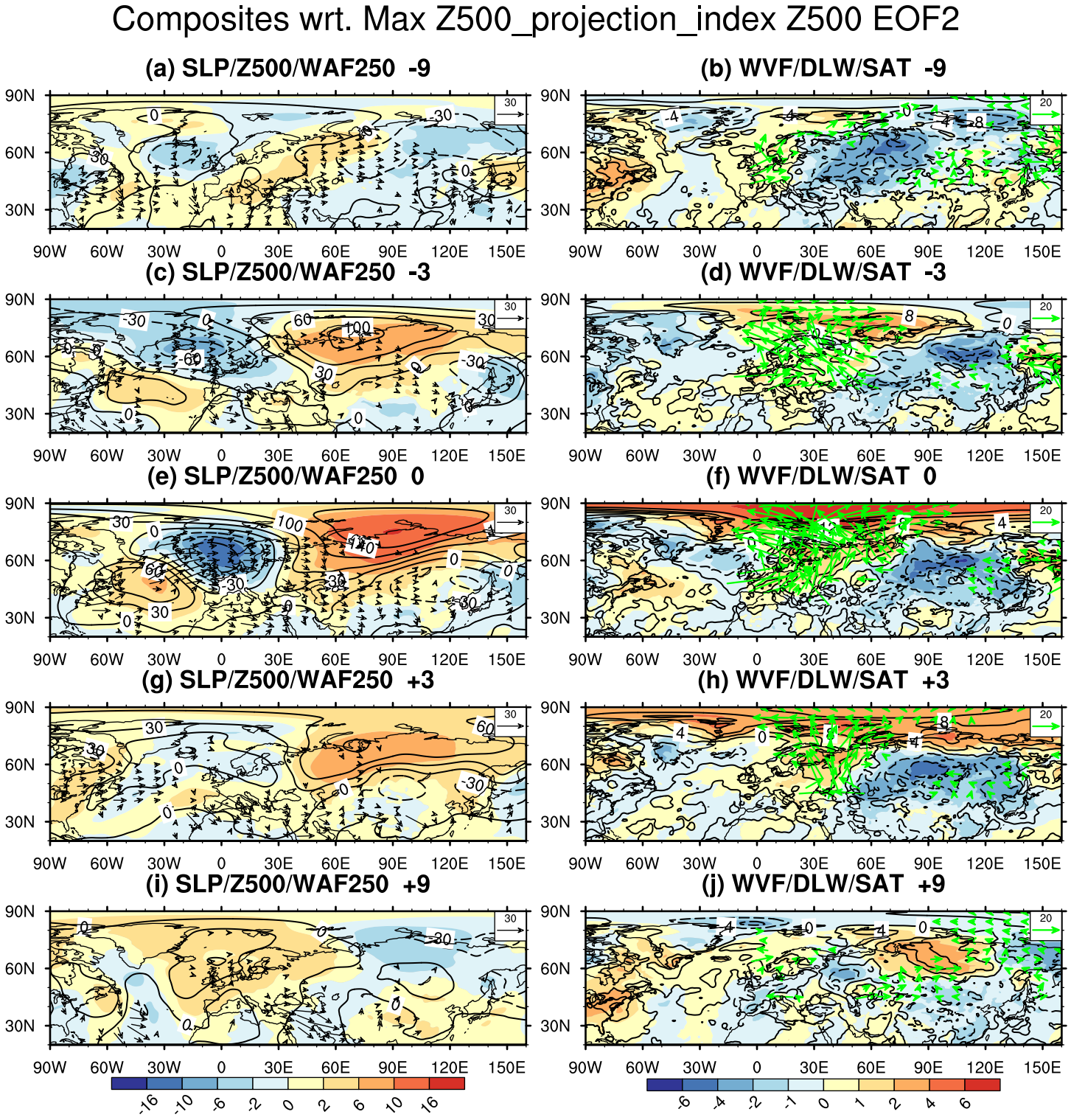

Figure S5. As in Figure 10, but using the filtered daily data. The seasonal-mean mean is also removed from each winter in the data.

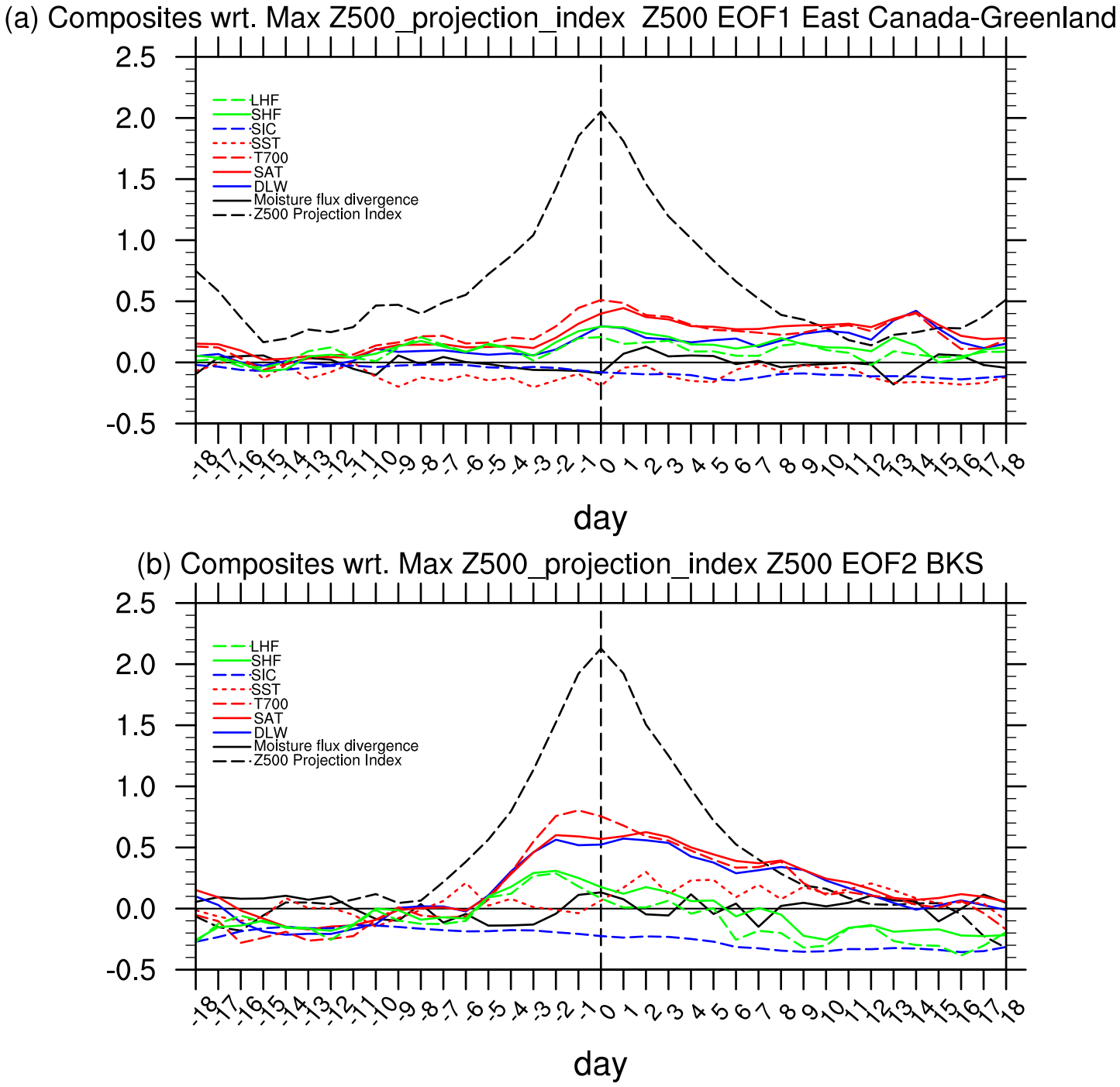

Figure S6. Similar to Figure 12, but with extended temporal range.

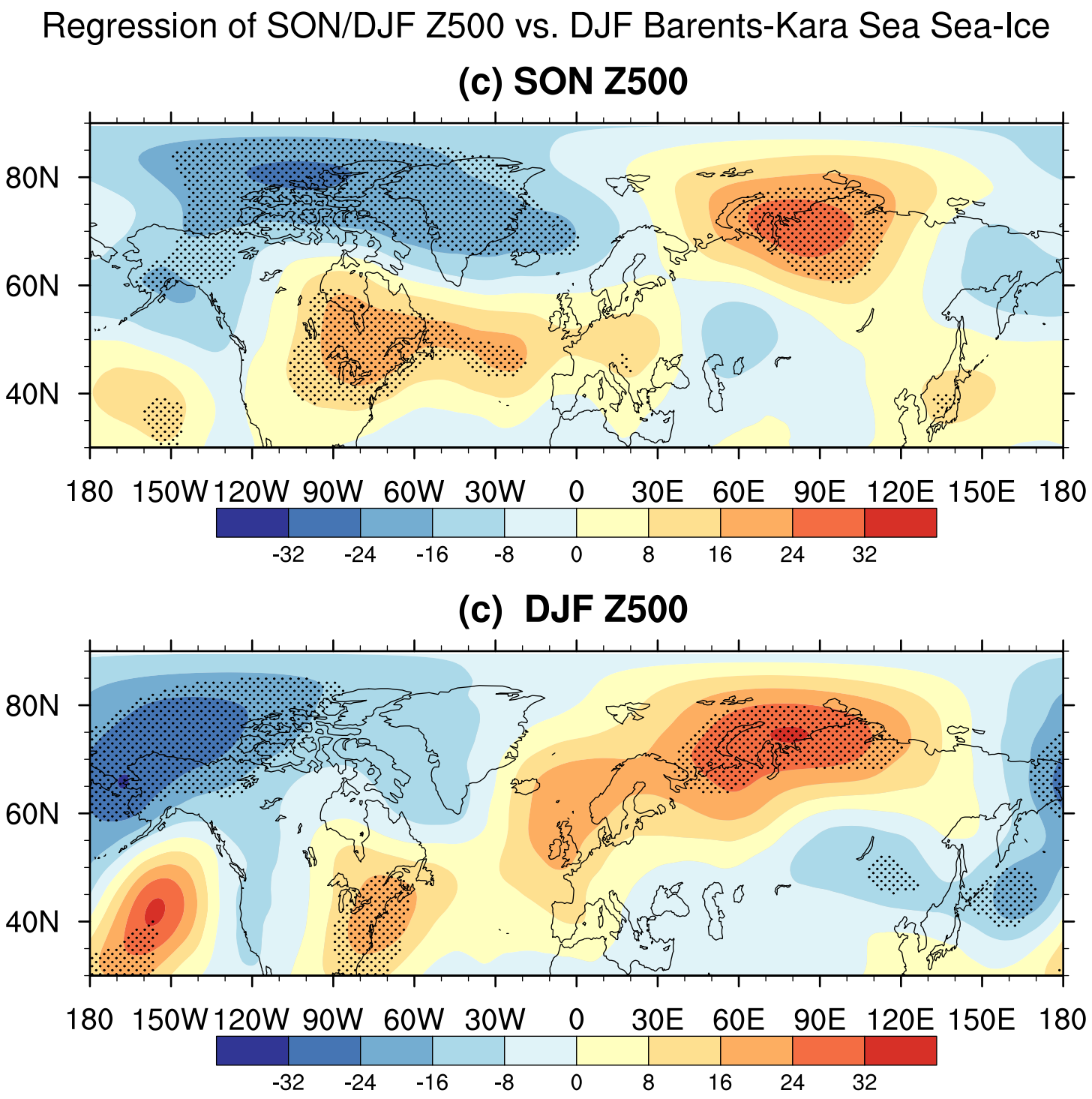

Figure S7. Regression coefficients of autumn/winter Z500 anomalies against the standardized winter BKS sea-ice. Sign of the regression coefficients is reversed to indicate the regression patterns corresponding to lower sea-ice conditions. Detrending (see Sect. 2a for definition) is applied to all the fields. Units: gpm. Stippling denotes regression anomalies significant at the 5% level.